/USA/ CR—96 — 207271

NAGW-4539

NAG5-4453

Structure of the magnetotail current sheet

Douglas J. Larson and Richard L. Kaufmann

Department of Physics, University of New Hampshire, Durham

Abstract. An orbit tracing technique was used to generate current sheets for three magnetotail models. Groups of ions were followed to calculate the resulting cross-tail current. Several groups then were combined to produce a current sheet. The goal is a model in which the ions and associated electrons carry the electric current distribution needed to generate the magnetic field **B** in which ion orbits were traced. The region $-20\,R_E < x < -14$ R_E in geocentric solar magnetospheric coordinates was studied. Emphasis was placed on identifying the categories of ion orbits which contribute most to the cross-tail current and on gaining physical insight into the manner by which the ions carry the observed current distribution. Ions that were trapped near $z = 0$, ions that magnetically mirrored throughout the current sheet, and ions that mirrored near the Earth all were needed. The current sheet structure was determined primarily by ion magnetization currents. Electrons of the observed energies carried relatively little cross-tail current in these quiet time current sheets. Distribution functions were generated and integrated to evaluate fluid parameters. An earlier model in which **B** depended only on z produced a consistent current sheet, but it did not provide a realistic representation of the Earth's middle magnetotail. In the present study, **B** changed substantially in the x and z directions but only weakly in the y direction within our region of interest. Plasmas with three characteristic particle energies were used with each of the magnetic field models. A plasma was found for each model in which the density, average energy, cross-tail current, and bulk flow velocity agreed well with satellite observations.

1. Introduction

Current sheets are present in the Earth's magnetotail, magnetopause and bow shock, and in many other space plasmas. The adiabaticity parameter is defined as $\kappa^2 = R_c/\rho_{zo}$, where R_c is the magnetic field line radius of curvature and ρ_{zo} is the gyroradius of an average current-carrying particle at $z = 0$, the center of the current sheet [*Büchner and Zelenyi*, 1989]. The criterion $\kappa < 1$ for the principal current-carrying particles may be used to define a thin current sheet. Such particles do not follow simple guiding center orbits. The principal distinction between the sheet-like structures studied here and a ring current is that the magnetic field in a current sheet must be generated by particles within the sheet. In contrast, the Earth's internal dipole dominates the magnetic field in the radiation belts. It therefore is necessary to consider local plasma currents to model the current sheet, while it may be possible to neglect local currents in the radiation belt. The goal of the present work is to investigate the physical structure of the thin current sheet in the Earth's magnetotail.

Consistent Orbit Tracing (COT)

Several methods have been used to construct models of the magnetotail. Each method uses a different set of basic assumptions and therefore provides different and often complementary insights into the physical structure of a current sheet. Simulations and some

orbit tracing methods involve injecting particles into a spatial region with fixed boundaries. Knowledge therefore is needed about the source of particles and the boundary conditions. Initial magnetic and electric field configurations within the region of interest are used to start a simulation, but detailed knowledge of these fields is only needed at the boundaries. Electric and magnetic fields are calculated self-consistently within the region of interest as the system evolves in time.

In contrast, the COT method requires that the basic magnetic and electric fields are known throughout region of interest. However, very little is assumed about particle sources or particle boundary conditions. Our selection of the COT technique was based on the assumption that the global magnetic field models give a good description of the magnetotail but that less is known about particle sources. One major limitation is that only steady state conditions can be studied.

The COT technique is equivalent to solving the Vlasov equation, so involves the motion of a noninteracting particle in a field generated by all other particles. Wave-particle interactions and instabilities are not considered in this treatment. The results presented here are confined to the region $-20\,R_E < x < -14\,R_E$, $0 < |z|$ $< 2\,R_E$ in geocentric solar magnetospheric coordinates. This region of interest was selected because AMPTE/IRM and ISEE 1 data were available. The major task in the COT procedure is to find a distribution of ions and electrons that will as nearly as possible generate the preselected magnetic field. In some respects the method is similar to a BGK solution [*Bernstein et al.*, 1957]. The BGK method is based on the assumption that a particle distribution can be found that will, through Poisson's equation, generate a wide variety of preselected electric field structures. The COT method is

based on the assumption that a particle distribution can be found that will, through Ampere's law, generate a variety of preselected magnetic field structures. If a realistic tail magnetic field model has been picked, then we assume that some distribution of ions and electrons with energies and densities similar to those measured in the tail can be found to produce this field.

The first step was to follow many ion orbits in the original magnetic and electric fields. The use of an error limit of 10^{-10} for trajectory tracing assures the inclusion of all nonguiding center effects. This detailed inclusion of orbital information is one of the strengths of the COT technique. Each group in the present study consisted of 1000 ions. Earthward drift was produced by a uniform dawn to dusk electric field. All current sheet ions were traced as they came in from tailward of the region of interest and drifted earthward completely through this region. No physical boundaries exist in the system except for the very rare particles that hit the Earth.

The cases described here started with monoenergetic ions. The angular characteristics of a biMaxwellian were used to randomly select an initial phase and pitch angle for each ion in the group. Ion energies change as particles drift in the electric field, but ions in each group remain in a fairly narrow energy band. Monoenergetic ions were used for this particular study because each such group tends to be dominated by particles that follow one of the orbit categories that are described below. A principal goal of the study was to find which orbit types are needed to produce a typical magnetotail current sheet. When Maxwellian or other broadly distributed ion groups are used, each group contains a mixture of ions following many different types of orbits. It therefore is harder to gain physical insight into the kinds of orbits that are needed to generate each model magnetic field.

As described later, a number of assumptions were introduced in order to add electron currents. The ion plus electron groups were then combined using a linear least squares fitting routine to find particles which will generate the preselected magnetic field.

One-Dimensional Results

The COT technique was used by *Kaufmann and Lu* [1993] to construct an approximately consistent one-dimensional (1-D) model magnetotail. Although orbits were traced in three dimensions, the model is referred to as a 1-D magnetotail because the modified Harris current sheet magnetic field was used [*Harris*, 1962]. The modified Harris model consists of a constant B_{zo} and a component $B_x(z) = B_{xo}\tanh(z/L)$ that varies only in the z direction.

Even though nearly consistent 1-D current sheets were found, the model did not provide a reasonable approximation to the magnetotail in our region of interest. The problems with the modified Harris model were that it required a density of several-keV ions that was higher than is observed, and it required streaming or anisotropies at the edge of the current sheet that were much larger than those observed. These are inherent problems with any consistent 1-D model of the middle magnetotail. An unrealistically high density is needed because there is no net cross-tail drift of trapped particles in a 1-D magnetic field [*Stern and Palmadesso*, 1975]. We were unable to generate modified Harris current sheets with typical magnetotail field strengths using ions and electrons with the energies observed unless the density was 1 cm^{-3} or larger. The average observed density in the $-20\,R_E < x < -14\,R_E$ region of interest is approximately 0.3 cm^{-3} [*Baumjohann et al.*, 1989; *Huang and Frank*, 1994b].

It is well known that streaming or a strong anisotropy, near the firehose instability limit, is needed at the edge of any 1-D current sheet to produce force balance [*Rich et al.*, 1972; *Cowley*, 1978]. The difficulty is that 1-D models have no x dependence, so require anisotropies much larger than those observed to balance the $\mathbf{j} \times \mathbf{B}$ force or equivalently, in a consistent model, the tension force of the sharply curved magnetic field lines. For these reasons, we concluded that no 1-D current sheet can produce a reasonable model of the middle magnetotail.

The present paper shows that the above problems are not present in a magnetic field model which has both x and z dependence. Section 2 describes the magnetic field models used, section 3 describes the ion orbits that exist in the model fields, and section 4 presents the basic COT results. Those fluid parameters that can be most directly compared to satellite measurements are discussed in section 5. Finally, section 6 summarizes the conclusions. Future papers will present the model distribution functions, analyze more complex fluid characteristics such as force balance and energy flow, and consider the question of uniqueness.

2. Tail Model

A simple magnetic field model was developed that provides a good representation of the portion of the tail being studied. A simplified model was needed to make accurate tracing of many ion orbits practical. The present study used a sum of fields from an Earth centered dipole, a ring current [*Tsyganenko and Usmanov*, 1982], an equilibrium or Harris-like tail field [*Birn et al.*, 1975; *Zwingmann*, 1983], and a uniform B_{zo}. Three-dimensional versions of the dipole and ring current fields were used so the mirroring of particles at low altitudes is as realistic as possible. The equilibrium tail field is 2-D, with B varying in the x and z directions.

The equilibrium tail field module is dominant in the region of interest. This module represents magnetic fields that are generated by approximately isotropic particle distributions. The specific form used was the one designated ZW by *Karimabadi et al.* [1990]. The dipole and uniform B_{zo} are vacuum fields, so require no electric currents in the magnetotail. The ring current is largely carried by particles earthward of the region of interest.

The dipole field was fixed for all versions of the model. Each of the other modules had parameters that were adjusted to generate a magnetotail with desired properties. Adjustments first were made so that the κ parameter and the total integrated cross-tail current would be similar to those at midnight in the $Kp = 4$ version of the much more complicated T89 [*Tsyganenko*, 1989] magnetosphere. An empirical magnetotail model tends to have a thicker current sheet than is present in the actual magnetotail. Waves and flapping of the tail broaden the apparent observed thickness obtained by binning satellite data. *McComas et al.* [1986], *Sanny et al.* [1994], and *Zhou et al.* [1995], using the ISEE 1 and 2 satellite pair, concluded that the typical instantaneous scale size of the principal current sheet is of the order of 1 R_E in our region of interest. We selected the $Kp = 4$ version of T89 to adjust κ because this version is thinner and has a larger equatorial B_z than the smaller Kp versions.

Figure 1 shows field lines in the noon-midnight meridian plane for the T89 model and the three simpler models used in the present study. Within the region of interest, characteristic scale lengths in the z direction for the cross-tail current j_y are about 0.3-0.4, 0.7, and 1.0 R_E in the models labeled thin, standard, and thick, respectively. The corresponding T89 scale length is about 1.2 R_E. In each
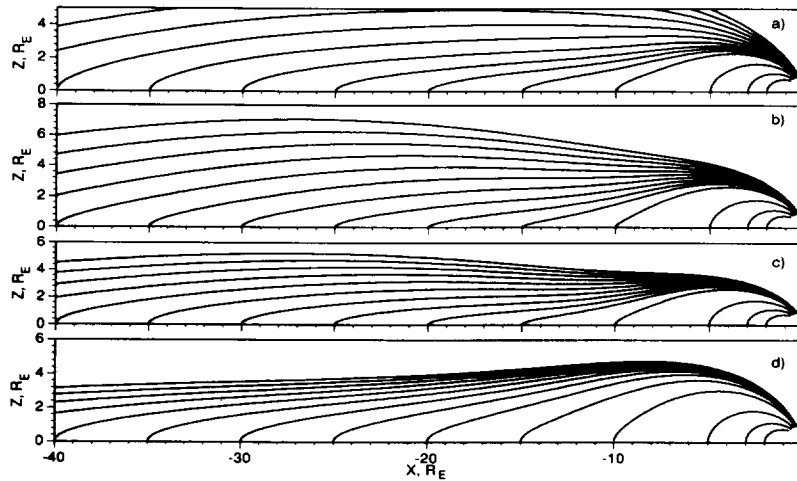
Figure 1. Magnetic field lines in the noon-midnight meridian plane for the (a) T89 with $Kp = 4$, (b) thin, (c) standard, and (d) thick magnetotail models.

case the current sheet thickness decreases by about 10% as one moves in from $x = -20$ to $-14\,R_E$.

The extra uniform B_{zo} term was included in our model so the magnetic field at $z = 0$ could be adjusted. For the standard model, B_z at the equator dropped from 5 nT at $x = -14\,R_E$ to below 3 nT at $x = -20\,R_E$. To get the same κ, the equatorial B_z dropped from 6 to about 3.5 nT in the thin model and from 4.5 to slightly above 2 nT in the thick model. This parameter is important in determining κ and the type of orbit that is dominant in any region of the tail.

Some uncertainty remains concerning the most appropriate equatorial B_z to select. *Huang and Frank* [1994a] defined the neutral sheet as the region with $|B_x| < 5$ nT in ISEE 1 data from 1978 and 1979. They found the average B_z to be approximately 7 nT in the region $-22\,R_E < x < -10\,R_E$. *Fairfield* [1986] used many years of data from the IMP 6, 7, and 8 satellites taken within $\pm 3\,R_E$ of the estimated location of the neutral sheet. Data were divided into one group for $-20\,R_E < x < -10\,R_E$ and a second group that extended from $x = -20\,R_E$ to the apogee of each satellite. This study found B_z as large as 7 nT to be uncommon in the lower altitude range, and extremely rare beyond 20 R_E. *Rostoker and Skone* [1993] used consistent methods to select only clear neutral sheet crossings in ISEE 1 data for $-22\,R_E < x < -10\,R_E$ and in IMP 8 data for $-38\,R_E < x < -22\,R_E$. Their Figure 3b shows a discontinuous drop in B_{zo} at $x = -22\,R_E$, which they suggested may partly be attributable to observations at different phases of the solar cycle. A corresponding average B_z has not been determined for the 1985 and 1986 AMPTE/IRM data sets we have used. *Nakamura et al.* [1991] selected a group of neutral sheet crossings by requiring $|\mathbf{B}|$ to drop below 5 nT. Since the observations with which we will make initial distribution function comparisons were selected from this group of neutral sheet crossings, most have B_z in the range that was used in the simple models. However, *Nakamura et al.* [1991] noted that the estimated uncertainty of the measured B_z is 1 nT while other components of $\mathbf{B}$ have uncertainties of only 0.1 nT in AMPTE/IRM data. This is because the satellite spin axis, along which magnetic field calibration is most difficult, lies close to the solar magnetospheric z direction.

3. Orbit Types

Ion orbits in the magnetotail usually are classified according to the particle's dynamical characteristics, for example, a chaotic, a resonant, or a guiding center orbit [*Chen*, 1992]. Particle dynamics are strongly dependent upon κ. However, the cross-tail current pattern carried by ions in the κ range studied here was found to be more dependent upon the particle's mirror point location than upon the dynamic orbital characteristic. Since a primary goal was to study the structure of a consistent current sheet, this paper categorizes orbits into three groups according to mirror points. We first define $z_o = mv/\,[qB_x\,(z_o)\,]$, which is the point at which the radius of curvature in the y-z plane of a particle with mass m, charge q, and velocity v is equal to the particle's distance from the equatorial plane. The first distinctive category consists of meandering and other trapped particles, which return to the equatorial plane without moving beyond $|z| = 2\,z_o$. Particles that magnetically mirror within the principal current sheet at $2\,z_o < |z| < 2\,R_E$ comprise the second category. These are sometimes called cucumber orbits [*Büchner and Zelenyi*, 1989]. Finally, the third category involves particles that mirror closer to the Earth. These are sometimes called Speiser orbits. The following section will show that some contribution from each of the above three orbit categories was needed to create a consistent current sheet that realistically approximated the Earth's magnetotail.

Sample Orbits

The sample orbits in this section show the physical manner in which particles carry cross-tail current in the standard tail model (Figure 1c). Magnetization currents are dominant for particles that mirror inside the current sheet [*Bird and Beard*, 1972; *Kaufmann and Lu*, 1993]. The x-z and x-y projections of the proton trajectory in Figures 2a and 2b show all three orbit categories. This proton had 5 keV of energy and was located at $(x, y, z) = (-18.5, 0, 0.5)\,R_E$ when tracing started. The ion mirrored once within the northern hemisphere of the current sheet as it drifted earthward from the starting point, became briefly trapped at $|z| < 2\,z_o = 0.5\,R_E$ near $x = -16$ to $-18\,R_E$, and then mirrored three times in the southern hemisphere. The first of these three southern hemisphere mirror points was within the principal current sheet and the other two were closer to the Earth. The orbit then was traced backward in time from the starting point, showing that this proton also had been trapped between $x = -29$ and $x = -20\,R_E$. This alternation between periods of being trapped near $z = 0$ and periods of magnetically mirroring at various points is typical of chaotic orbits [*Ashour-Abdalla et al.*, 1995].
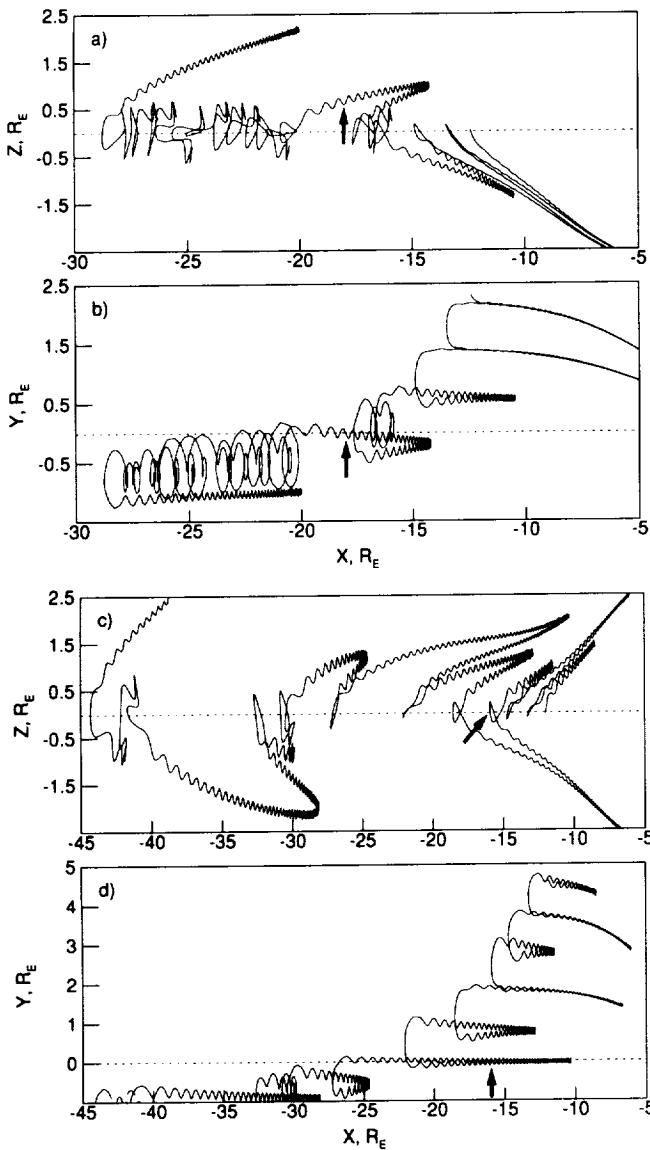
Figure 2. (a), (b) Two projections of one proton orbit in the standard magnetotail model. Tracing started with a 5-keV proton at (x, y, z) = (-18.5, 0, 0.5) R_E. (c), (d) Tracing started with a 5-keV proton at (-16.5, 0, 1.5) R_E. The arrows point to the starting locations.

Since the $-20\,R_E < x < -14\,R_E$, $0 < |z| < 2\,R_E$ region was being investigated, orbit tracing was stopped on the earthward side when the ion crossed $z = 0$ at a point at least 2 gyroradii earthward of $x = -14\,R_E$. Similarly, tracing backward in time was stopped when the ion crossed $x = -20\,R_E$ at least 2 gyroradii beyond $|z| = 2\,R_E$. An equatorial crossing tailward of the field line that connects to $x = -20\,R_E$, $|z| = 2\,R_E$ plus 2 gyroradii also can be used to stop back tracing. It is evident from Figure 2 that no specific particle boundary conditions were imposed at the edges of the region of interest, and that nothing unusual happened at the starting position. Starting points were selected to get groups of ions that were dominated by a particular trajectory type. For example, starting the ions with an isotropic distribution at $z = 0$ gives a group that begins with many trapped ions, while no ions that start at large $|z|$ are initially trapped.

Cross-Tail Drift and Current

Figures 2b and 2d show the physical manner by which the bounce averaged cross-tail drift becomes relatively independent of

the details of a trajectory and of deviations from guiding center motion. Figure 2 also shows the most important differences between orbits in 1-D and either 2-D or 3-D models. Note that during the last two orbit segments in Figure 2b, when the mirror point was below $x = -10\,R_E$, the particle followed almost the same field line as it moved down to and back from a mirror point. The same feature is evident in Figure 2d whenever the ion mirrored below 10 R_E. Protons mirroring near the Earth with energies of about 5 keV in this magnetic field appear to simply bounce off the current sheet [*Speiser*, 1965] when they reach the equator (Figure 2a). Mirror points on the orbits immediately before and after a given current sheet interaction are nearly the same if the particle's κ parameter is close to a resonant value [*Büchner and Zelenyi*, 1989; *Chen*, 1992]. The mirror points of chaotic particles, with κ well removed from the resonant values, generally are different after each current sheet interaction. However, in this paper all resonant and chaotic particles that mirror near the Earth are placed into the same category because the cross-tail current distribution in the region of interest is similar for these two dynamically different trajectory classes. Whenever the mirror point is near Earth, the total cross-tail displacement achieved in one bounce cycle is approximately equal to 2 gyroradii based on B_{zo}. Note that different scales are used for the x, y, and z axes in Figure 2, so that circular motion near $z = 0$ appears to be stretched in the y direction. The motion of particles that mirror at low altitudes in 2-D and 3-D models is similar to the motion of untrapped particles in a 1-D model. In all these cases, j_y is concentrated in a sheet near $z = 0$ that is much thinner than is required to consistently generate the standard model magnetotail.

Figure 2b shows that this ion drifted part way back in the negative y direction when it mirrored within the current sheet, near $z = -1.5\,R_E$, $x = -10\,R_E$ and near $z = 0.7\,R_E$, $x = -14\,R_E$. In both cases there was a substantial net cross-tail drift during a full bounce cycle. Similar bounce cycles are seen in Figure 2d. The fact that all trapped and mirroring ions undergo a net cross-tail drift during each bounce cycle is one of the most important differences between either 2-D or 3-D and 1-D models. In the 1-D models, where both the x and y components of the canonical momentum are conserved, all mirroring particles drift equal distances in the $+y$ direction near $z = 0$ and in the $-y$ direction as they mirror. Self-consistent 2-D and 3-D models have lower total plasma densities than 1-D models because particles that mirror within the current sheet carry a net cross-tail current in the x dependent models.

Particles of species s that obey the guiding center equations in a gyrotropic plasma carry a current given by

$$\mathbf{j}_{s\perp} = \frac{\mathbf{B}}{B^2} \times \left[\nabla P_{s\perp} + \frac{P_{s\parallel} - P_{s\perp}}{B^2} (\mathbf{B} \cdot \nabla) \mathbf{B} \right] + n_s q_s \frac{\mathbf{E} \times \mathbf{B}}{B^2} \qquad (1)$$

This current involves both drifts of the guiding centers $\mathbf{v}_g$ and a divergence-free magnetization drift $\mathbf{v}_m$. The small polarization drift has been neglected. The drift $\mathbf{v}_g$ is a combination of gradient, curvature, and $\mathbf{E} \times \mathbf{B}$ drifts. Curvature guiding center drift is associated with the $P_{s\parallel}$ factor in (1). The curvature guiding center drift is large and positive near $z = 0$. The first $P_{s\perp}$ factor in (1) represents temperature and density gradient magnetization currents, and the second $P_{s\perp}$ factor in (1) is the curvature magnetization current or orbit crowding effect. The magnetic field gradient produces both a drift of guiding centers in the $+y$ direction near $z = 0$ and a magnetization current in the $-y$ direction. No magnetic field gradient term appears in (1) because the associated guiding center $\mathbf{v}_g$ and magnetization $\mathbf{v}_m$ terms cancel.

Figure 2b shows that there is a small cross-tail drift per current sheet interaction during the periods when the ion was trapped at |z| < 0.5 R_E, beyond $x = -20$ R_E. This helps to explain why the bounce-averaged drift velocity depends relatively weakly on orbit type. Trapped particles make many current sheet interactions, but have a net cross-tail displacement per interaction that is much less than 2 gyroradii. Particles mirroring near the Earth have few current sheet interactions, but have a net displacement of nearly 2 full gyroradii during each interaction.

Figures 2c and 2d show another important property of magnetotail current carriers. This trajectory is characterized by a series of events in which the ion mirrors and then interacts briefly with the current sheet. The cross-tail motion tends to increase modestly during each current sheet interaction as the ion moves into the inner tail because the ion is gaining energy. However, it is more important that the earthward drift speed is decreasing at low altitudes. The ion moves earthward by as much as 10 R_E during the time required to mirror when its equatorial crossing point is near $x = -30$ to -40 R_E. Earthward motion is only about 1 R_E per mirror cycle near $x = -10$ R_E. This decrease in earthward drift is the primary reason that the displacement between adjacent equatorial crossing points is mostly in the x direction in the distant tail and mostly in the y direction in the near-Earth tail. The result is an Alfvén layer or wall [*Ashour-Abdalla et al.*, 1992]. A group of particles from a deep-tail source with a given average magnetic moment do not penetrate to lower field lines.

Figures 3a, 3b, and 3c show x-z, x-y, and y-z plots of a proton that started at $(-15.5, 0, 1.0)$ R_E with 15 keV of energy. This high energy proton passed through both the $N = 1$ and $N = 2$ resonances.
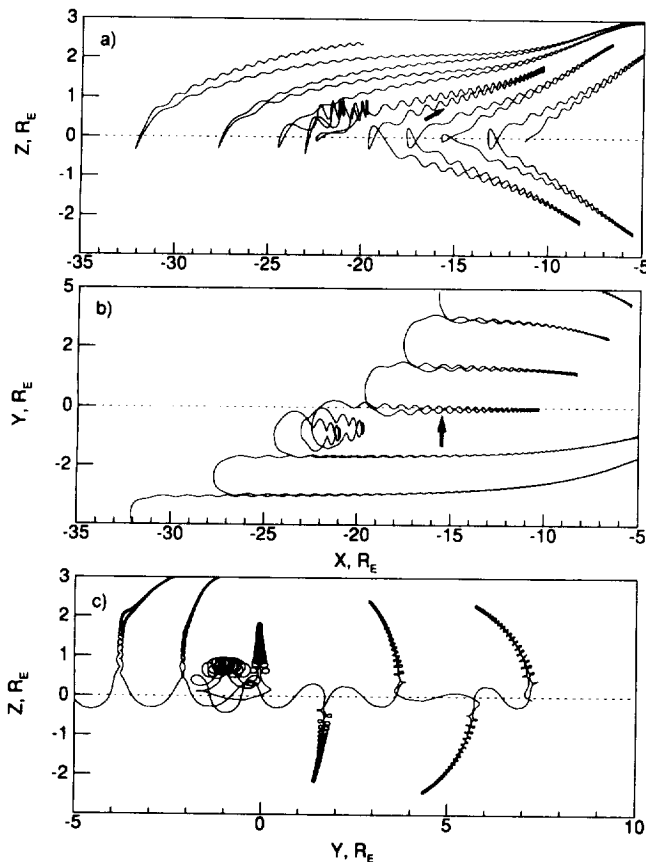

Figure 3. Three projections of one proton orbit in the standard magnetotail model. Tracing started with a 15-keV proton at $(-15.5, 0, 1.0)$ R_E.
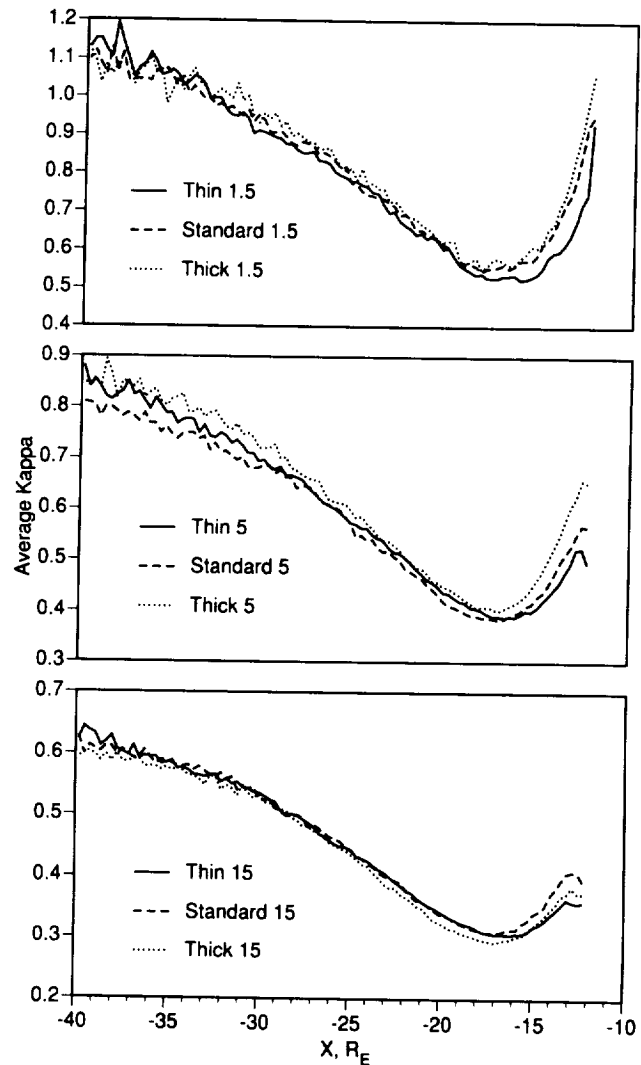

Figure 4. Average κ for ions in the nine runs. The κ parameter was calculated every time a particle crossed equatorial plane. Each panel shows results for one starting energy: 1.5, 5, or 15 keV. Energies change as the particles drift.

Resonances are characterized by symmetric orbits that involve little net change in magnetic moment. A particle's magnetic moment changes dramatically near the halfway point between resonances. A resonant ion crosses the $z = 0$ plane $N+1$ times during each current sheet interaction [*Büchner and Zelenyi*, 1989]. An individual particle in the tail is accelerated as it drifts earthward and duskward. Acceleration tends to increase ρ_{zo} and therefore to reduce κ for the particle. However, κ tends to increase when the particle reaches the more dipolar field lines with large R_c in the inner tail. Figure 4 shows that these two competing effects lead to a minimum κ near $x = -17$ R_E in our models for all starting energies used. The κ parameter of the particle in Figure 3 decreased from a little more than 0.5 at the $x = -32$ R_E crossing, which lies near the $N = 1$ resonance, to about 0.3 at -15 R_E, which is near the $N = 2$ resonance. Note that the ion crossed $z = 0$ twice during each of the two most distant neutral sheet interactions before it became briefly trapped, and then crossed $z = 0$ three times during each of the four most earthward interactions. The magnetic moment and the mirror magnetic field changed substantially during the crossings at -25 R_E < x < -20 R_E when κ was near 0.4. This behavior is typical of highly chaotic motion halfway between resonances.

Figures 5a, 5b, and 5c show x-z, x-y, and y-z trajectory projections for a proton that started with 15 keV of energy at (-14.5, 0, 0). Although it is unusual to last this long, the orbit shows that it is possible for a proton to remain trapped in a very simple pattern as it drifts earthward all the way from $x = -30\ R_E$ to $x = -15\ R_E$. The κ parameter changed substantially in this interval. This orbit is referred to as a figure eight pattern because of its appearance in the y-z projection. By following one cycle of the figure eight pattern in Figure 5c, it is particularly easy to see that this ion always moves in the $+y$ direction at $|z| > 0.3\ R_E$ and in the $-y$ direction at $|z| < z_0$. Although not as obvious, all groups of trapped ions carry a similar current distribution.

4. Generation of Model Current Sheets

This section presents sample results from nine runs using the COT technique. The thin, standard, and thick magnetotail models were each used for three runs. For each magnetotail model, one plasma sheet was generated using monoenergetic 1.5 keV, one using 5 keV, and one using 15 keV starting proton energies. Ions are energized as they drift in the uniform $E_y = 0.3$ mV/m or 1.9 kV/R_E electric field. However, the ions in an initially monoenergetic group remain concentrated in a relatively narrow energy band at any one location, so that a single orbit type tends to dominate.

Distribution Functions

The calculations used twenty 0.1-R_E thick z boxes in the range 0 < $|z|$ < 2 R_E. The model is symmetric about $z = 0$, so orbital infor-
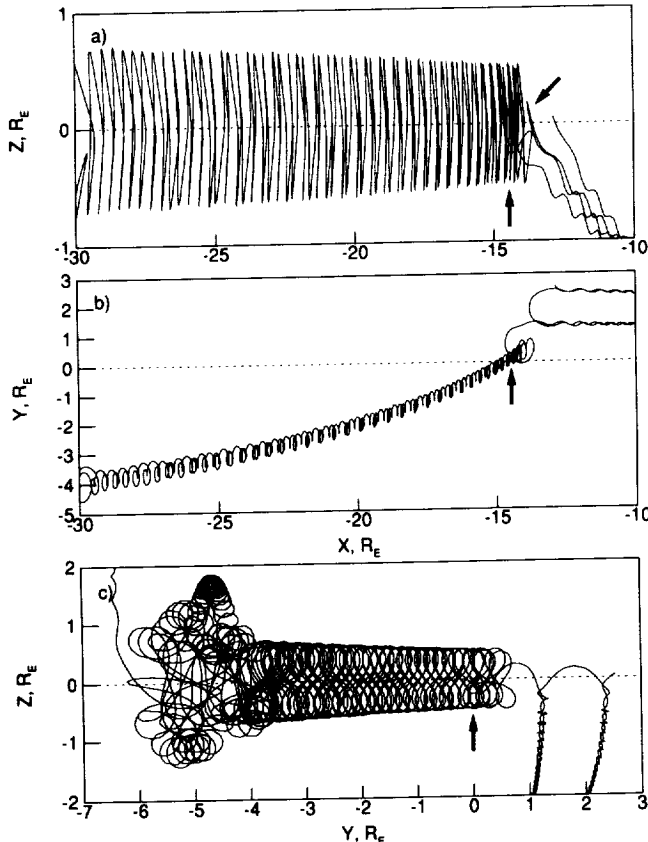

Figure 5. Three projections of one proton orbit in the standard magnetotail model. Tracing started with a 15-keV proton at (-14.5, 0, 0) R_E.

mation at equal distances above and below $z = 0$ were combined in these 20 boxes. Six 1-R_E wide x boxes in the range $-20\ R_E < x < -14\ R_E$ were used at each z. Since there is very little y dependence in this region of interest, only one y box extending to $y = \pm10\ R_E$ was used. As a result, distribution functions were generated for a total of 120 spatial boxes. We refer to this set of runs as two dimensional because of the lack of significant y dependence even though all calculations and binning are fully three dimensional. Although no useful information would be gained by keeping multiple y boxes for the present runs, several y boxes are retained when either y dependence is added to the equilibrium tail module or when distribution functions are needed near or sunward of $x = -10\ R_E$.

Two methods were used to calculate the ion number density $n_i(x, z)$ and current density $j_i(x, z)$. The point at which each box was entered was determined accurately during orbit tracing. New orbit points were introduced at each box edge crossing point so that all orbit segments remained within one of the 120 spatial boxes. Use of the efficient Bulirsch-Stoer tracing algorithm made step sizes so large that linear interpolation was not adequate for the curved trajectories. The new techniques described below removed the anomalies at certain pitch and phase angles that were noted by *Kaufmann and Lu* [1993]. The most serious problem in our earlier study involved the generation of distribution functions by counting particles only when they crossed a plane surface. With large step sizes, the distribution functions generated by this method had anomalously low values when the velocity normal to the detector was small.

The first technique involved keeping track of the total time spent and the total distance that all particles in a group traveled in the x, y, and z directions while they were inside each box. Density is proportional to this time and $j_i(x, z)$ is proportional to the distance. *Eastwood* [1972] and *Kaufmann and Lu* [1993] described the use of this method. The resulting $j_i(x, z)$ includes all ion guiding center drift, magnetization, and nonguiding center currents.

For the second technique, velocity space was divided into 30 × 30 × 30 boxes in the v_x, v_y, and v_z directions. The result is a 27,000-point velocity distribution function for each of the 120 spatial boxes. The distribution functions were generated by adding the time spent when taking each step along a trajectory into two of the 27,000 × 120 velocity-spatial boxes, with half the time for each step placed into the initial and half into the final velocity box for this step. Integrating the distribution function gave essentially the same $n_i(x, z)$ and $j_i(x, z)$ as was obtained by the first method. Adding in the electron current, described below, gave the total $j(x, z)$ in each box.

Sample Case

A set of 30 groups of 1000 ions were traced for each of the nine cases noted above. The angular distributions all were selected so that $f(\mathbf{r}, \mathbf{v})$ would have been isotropic if the ions had started in a uniform $\mathbf{B}$. An actual $f(\mathbf{r}, \mathbf{v})$ may be anisotropic even in the starting box because ions can return to this box with different pitch angles. For any one of the nine runs, the 30 groups of ions all started with the same energy, which was 1.5 keV, 5 keV, or 15 keV. The only difference between the 30 groups in any one run was the location at which orbit tracing began. The starting points were $z = 0, 0.5, 1.0,$ and $1.5\ R_E$ at the centers of each of the six x boxes, plus at $z = 2.0$ on field lines that crossed the equator at the centers of each x box.

The three columns in Figure 6 show the cross-tail components of the ion, electron, and total ion-plus-electron group currents for the thick-5 keV case. Figures 6a through 6e show currents from
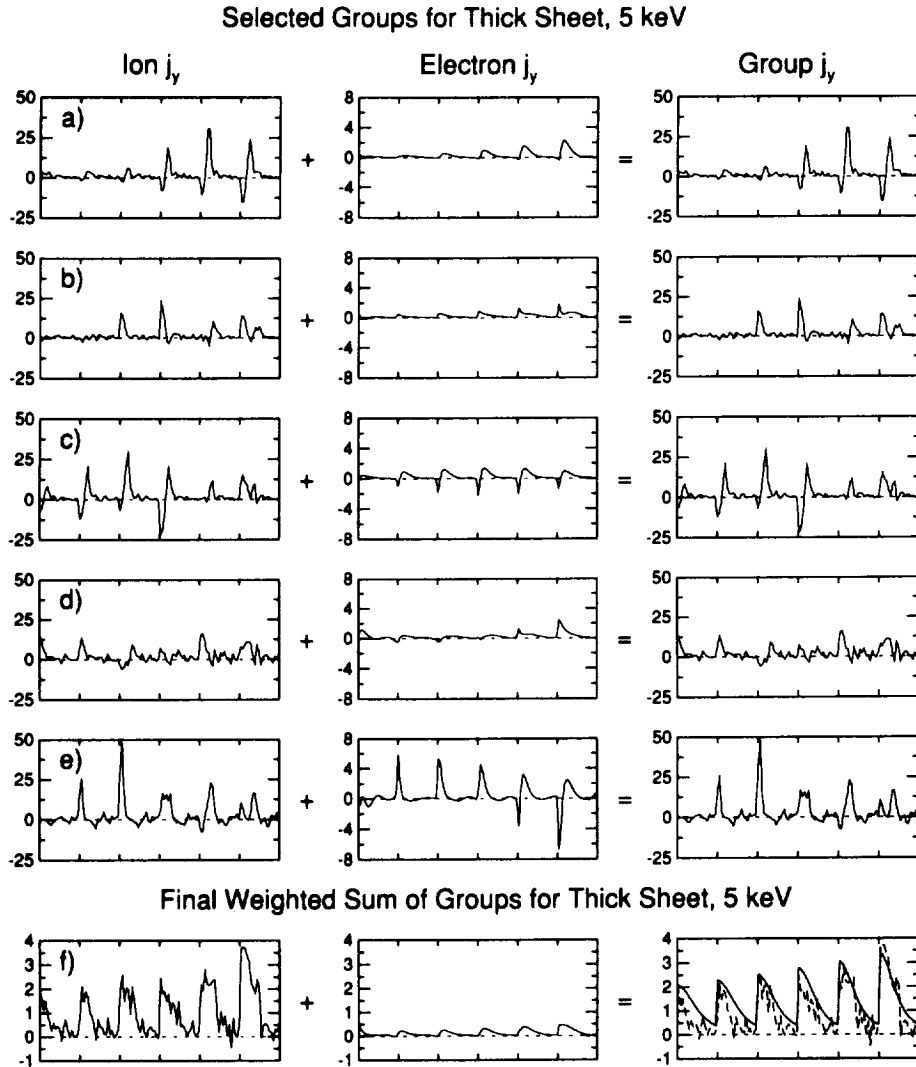
Selected Groups for Thick Sheet, 5 keV

Figure 6. (a) - (e) Cross tail currents carried by groups of 1000 ions, their accompanying electrons, and by the total ion-plus-electron groups. The thick magnetotail model was used. (f) Weighted sum of Figures 6a to 6e. The solid curve in the group j_y column is the current needed to produce a consistent magnetotail.

five groups of 1000 particles, and Figure 6f is a weighted sum of Figures 6a through 6e. For example, the ion j_y panel in Figure 6a shows the current carried by a group of 1000 ions that were started at $x = -15.5\ R_E$, $z = 0$. The smooth solid curve in the group j_y column of Figure 6f shows the cross-tail current that is needed to generate the model magnetic field.

The horizontal axis of each panel in this figure is divided by tick marks into six blocks associated with the six different x boxes. The block at the left side of each panel, labeled −19.5, includes all information for the range $-20\ R_E < x < -19\ R_E$. The block at the right side of each panel, labeled −14.5, corresponds to $-15\ R_E < x < -14\ R_E$. Within each x block are 20 points representing increasing z values in the range $0 < |z| < 2\ R_E$. The smooth curve in the group j_y column of Figure 6f shows that the j_y (x, z) which is needed to generate **B** is largest at $z = 0$ in each x box, and drops monotonically as z increases to $2\ R_E$. This panel also shows that larger currents are needed in x boxes closer to Earth. The 5-keV row in Figure 7 shows the same information as is in the group j_y panel in Figure 6f. The six x boxes are plotted separately and labeled more completely in Figure 7.

A number of assumptions were made to calculate the current carried by Maxwellian electrons. Most of these assumptions have already been described because they were used in the 1-D calculations [*Kaufmann and Lu*, 1993]. A polynomial fit was made to both $n_i\ (x, z)$ and the average ion energy for each group traced. The electron number density $n_e\ (x, z)$ was set equal to the polynomial fit to $n_i (x, z)$ so the resulting plasma would be approximately neutral. Since n_e would be constant along field lines if electrons were isotropic at the equator, a first-order parallel electric field was added to the zeroth-order uniform E_y. The Boltzmann relation

$$n_e(x, z)\ =\ n_e(x_o, z_o)\ \exp\ [-q_e\phi/T_e] \qquad (2)$$

was used to calculate the electric potential difference ϕ between each (x, z) box and a reference point (x_o, z_o) on the same field line. The average electron energy or $3/2\ T_e$ was taken to be $1/7$ of a polynomial fit to the ion group average energy [*Baumjohann et al.*, 1989]. Since electrons are much less energetic than ions, electrons were influenced much more strongly by the parallel electric field than were ions. Equation
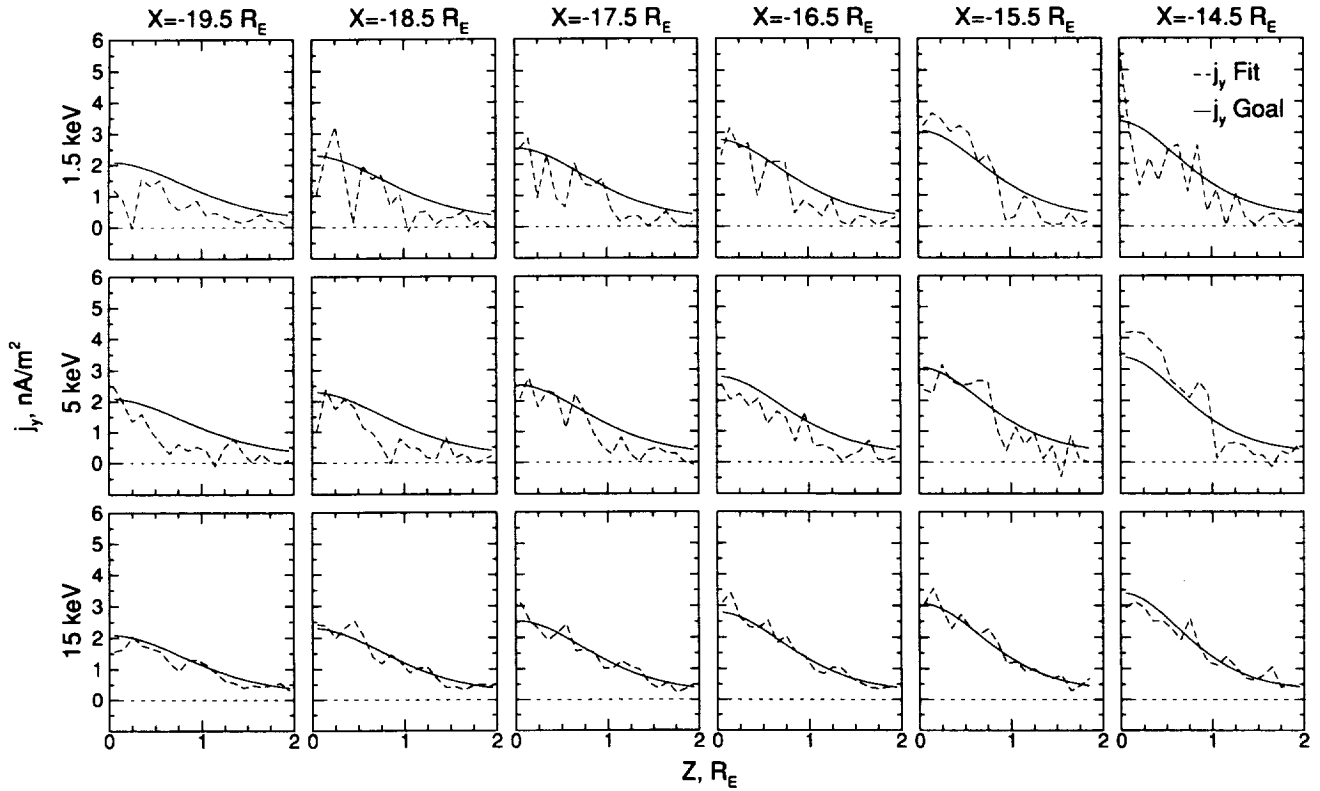
Figure 7. Solid curves are the cross-tail currents need to produce the thick model current sheet. Each column corresponds to a 1-R_E thick x box. Dashed curves are the least squares fits obtained by adding currents carried by five to nine groups of 1000 ions and electrons. There are 20 points along the horizontal axis in each panel, corresponding to the 20 z boxes. The three rows of panels were produced by starting protons with 1.5, 5, or 15 keV of energy, as indicated.

(2) only gives the distribution of ϕ along a field line, so only determines the parallel electric field. Since $E_\parallel$ is distributed differently along adjacent field lines, some $E_\perp$ in the x-z plane must also be present. We used a variational approach to determine this $E_\perp$. It was assumed that $E_\perp$ will develop so that the energy density $\varepsilon_o E^2$ is minimized. This assumption completes the definition of **E**. The total potential drop between $z = 0$ and $z = 2\, R_E$ was no more than 200 V. This potential difference is similar to the values obtained in our previous 1-D model. Some groups of ion orbits were traced again in the magnetic field with this added $E_\parallel$. The small potential drop had very little effect on the ion $j_y(x, z)$ distribution.

The κ for each group of electrons is 11 times the κ for the associated proton group, so all electron motion is well approximated by the guiding center assumptions in the models studied here. The electron cross-field current was calculated from (1) based on the polynomial fits to $n_e(x, z)$ and an isotropic $P_e(x, z) = n_e T_e$. This procedure yielded the electron $j_y(x, z)$ for each group, as shown in the middle column of Figure 6. The addition of electron and ion currents gave the total $j_y(x, z)$ for each group, as shown in the right column of Figure 6.

The above procedure, which assumes isotropy and the presence of $E_\parallel$, is not the only one that could be used to include electrons. Instead, it is possible to produce charge neutrality along field lines with $E_\parallel = 0$ by adjusting the angular distribution of electrons at the equator. Substantial electron anisotropies involving $T_\parallel > T_\perp$ have been observed in the central plasma sheet [*Hada et al.*, 1981; *Paterson et al.*, 1995], though most observations have reported approximate isotropy at $z = 0$. In the guiding center approximation,

a biMaxwellian distribution at the equator yields a density variation along a field line of

$$n(B) = \frac{n_o T_\parallel}{T_\perp + (T_\parallel - T_\perp)\,(B_o/B)}\, \exp\,[-q\phi/T_\parallel] \qquad (3)$$

where n_o and B_o are the particle density and |**B**| at the equator. When $E_\parallel = 0$ or $\phi = 0$ everywhere, the density varies by a factor of $T_\parallel/T_\perp$ as one moves from the equator to the ionosphere.

When the particle density is known all along a field line, it is possible to calculate the angular distribution needed for charge neutrality with $E_\parallel = 0$ throughout the region where the guiding center equations are valid. However, we retained density information only in the previously defined region of interest, so do not have densities all the way down to the ionosphere. One model in which the ion density changes rapidly along a field line will be shown later. An electron distribution with very abrupt pitch angle variations would be needed to maintain charge neutrality in this case if $E_\parallel = 0$. The method used in the present analysis is easy to implement and results in reasonable distribution functions for all cases studied. Since electron cross-tail currents are small in sheets with the thicknesses used here, this simple method should be adequate.

Current Distributions

It is clear that none of the individual groups shown in Figure 6a-6e carried a current distribution that is even remotely similar to the current needed for self-consistency. This observation was valid

for each of the 30 groups of particles traced in each of the nine cases studied. However, a weighted sum of several groups often can produce a reasonable approximation to the necessary $j_y(x, z)$. The final current density obtained by linearly combining the five groups in Figure 6a-6e is shown by the dashed line in the group j_y panel of Figure 6f and in the 5-keV row of Figure 7.

Current distributions produced by the individual ion groups in the ion j_y column of Figure 6 show the typical patterns that were described qualitatively in the discussion of individual orbits. For example, many figure eight and other trapped orbits appear in the group of particles shown in Figure 6a, which started at $z = 0$ at $x = -15.5 R_E$. This is the second of the six x blocks from the right. The resulting ion current shows the typical trapped particle signature involving negative j_y at $z = 0$ and positive j_y beyond z_o, which is near or below 0.3 R_E for 5 keV protons in the region of interest. The above current pattern is dominant in the starting and adjacent x boxes (three rightmost blocks in the panel) because many particles remain trapped for only a few current sheet interactions. Similarly, the ion j_y panel in Figure 6c shows the current carried by ions that started at $z = 0$, $x = -17.5 R_E$. The characteristic trapped particle $j_y(x, z)$ pattern here appears in the more distant x boxes (blocks on the left side).

There is a net drift of all trapped ions in the positive y direction, as noted previously. The net positive current can be seen in Figures 6a and 6c because the area under the positive j_y spikes is a little larger than the area under the negative spikes. However, the structure of $j_y(x, z)$ clearly is dominated by the sharp positive and negative peaks, which are associated with magnetization currents, rather than by a small relatively uniform positive j_y at $|z| < 0.5 R_E$ that would be predicted by (1) for an isotropic distribution.

Ions in Figure 6e were started at $z = 2 R_E$ on a field line that crosses the equator at $x = -19.5 R_E$. These ions all have initial mirror points outside the current sheet. The ions carry cross-tail current that is strongly confined near $z = 0$ when they first bounce off the current sheet, in x boxes near the left side of the ion j_y panel in Figure 6e. The current is less well confined during succeeding bounces at lower altitudes because some ions mirrored closer to $z = 0$ or became trapped. In addition, ions with low altitude mirror points usually have drifted several Earth radii earthward before they return to $z = 0$. This $j_y(x, z)$ structure is typical of any group of particles that is selected to be generally isotropic far from $z = 0$, regardless of the particle's κ or dynamical characteristics. The principal difference between particles on chaotic and resonant orbits is that resonant particles would maintain low mirror points for several bounces, so the pattern of narrow regions with strong positive j_y would be more extended in the x direction. A chaotic particle group would not continue to be dominated by particles with low mirror points after one or two current sheet interactions.

Figures 6b and 6d show currents carried by ions that started with an isotropic distribution at $z = 0.5 R_E$, with $x = -15.5$ and $-17.5 R_E$ respectively. These groups are dominated by ions which mirror somewhere in the outer portion of the current sheet, beyond $z = 0.5 R_E$. The associated j_y patterns tend to be complex, but are reproduced by other randomly selected groups of 1000 ions, even down to small details. Trapped ions with mirror points throughout the current sheet are needed to broaden the current carried by 5-keV protons so they can produce a sheet that is thicker than the region associated with meandering orbits.

As noted above, none of the individual ion groups has a j_y structure that is similar to the goal, as shown by the solid curves in the group j_y panel of Figure 6f and in the 5-keV row of Figure 7. For example, the low mirror point group (Figure 6e) produces much

too thin a current sheet. However, if some of the trapped particle group currents (Figures 6a and 6c) are added, it will decrease the positive current very close to $z = 0$ and add some positive current at larger $|z|$. This is the procedure used in the COT technique, as described previously [Kaufmann and Lu, 1993].

A linear combination using all 30 particle groups that were traced for each of the nine cases studied would yield the best least squares fit to the $j_y(x, z)$ that is needed to generate a consistent magnetic field. However, a principal goal of this study was to see which orbit types were essential for the production of a consistent current sheet. For this reason, only those groups that improved the fit at a 95% confidence level were retained. Positive weighting coefficients were required for each group. Of the 30 groups generated for each case, no more than nine and no fewer than five groups were selected after imposing these requirements. The thick 5-keV case shown in Figure 6 was used as an illustration, even though the final fit was one of the poorest, because it was the one with the fewest groups in this final fit.

Figures 7-9 show how closely the model $j_y(x, z)$ compares to the desired $j_y(x, z)$ that is needed for self-consistency for each of the nine cases studied. This is the most critical step in the COT procedure, and the validity of the technique depends upon our ability to find consistent solutions which also agree with observations for nearly all preselected current sheet structures. The existence of a permanent current sheet in the magnetotail suggests that it is possible to find some such distribution of particles, though not necessarily with groups of particles which all have the same starting energy. The jaggedness of the nine least squares fits is a consequence of the summation of only five to nine nearly monoenergetic particle groups. Smoother results are obtained in other runs using Maxwellian distributions and distributed injection points.

The 15-keV results in Figures 7-9 show good agreement with the required j_y for all three magnetic field models. However, average ion energies are observed to be closer to 5 keV in the typical quiet magnetotail. The thin and standard magnetic field model results using 5-keV starting energies yielded j_y that is in reasonable agreement with that needed for consistency (Figures 8 and 9). However, we did not find 5-keV ion groups that carried j_y over a sufficiently broad range in z to match the currents needed in the thick model at large $|x|$. Problems in finding $j_y(x, z)$ that have the desired z dependence also are evident in the 1.5-keV results, particularly beyond $x = -17 R_E$.

Part of the fitting problem may be associated with our use of the equilibrium tail module as the dominant contribution to the magnetic field in our region of interest. The module was selected because it is known that this field can be generated by an isotropic distribution function. However, the distribution functions from which the entire set of equilibrium tail modules were derived contain unrealistic properties. One property that is in disagreement with observations is the uniform cross-tail drift velocity at all x and z that is assumed when deriving the equilibrium modules [Harris, 1962; Schindler, 1972; Kan, 1973]. In contrast, observations and our COT results have the largest v_y near $z = 0$. Burkhart and Chen [1993] pointed out the unrealistic thickening of the distant tail current sheet in this set of models. The complete fields, which have been produced by selecting parameters and adding several modules to fit T89 (Figure 1), do not show a dramatic thickening. Nevertheless, the difficulty in finding ions which will generate a thick enough current sheet in the more distant portion of our tail models may be associated with this unrealistic property of the equilibrium tail module. A final unrealistic assumption used when developing the equilibrium tail module was that a frame exists in which $E = 0$

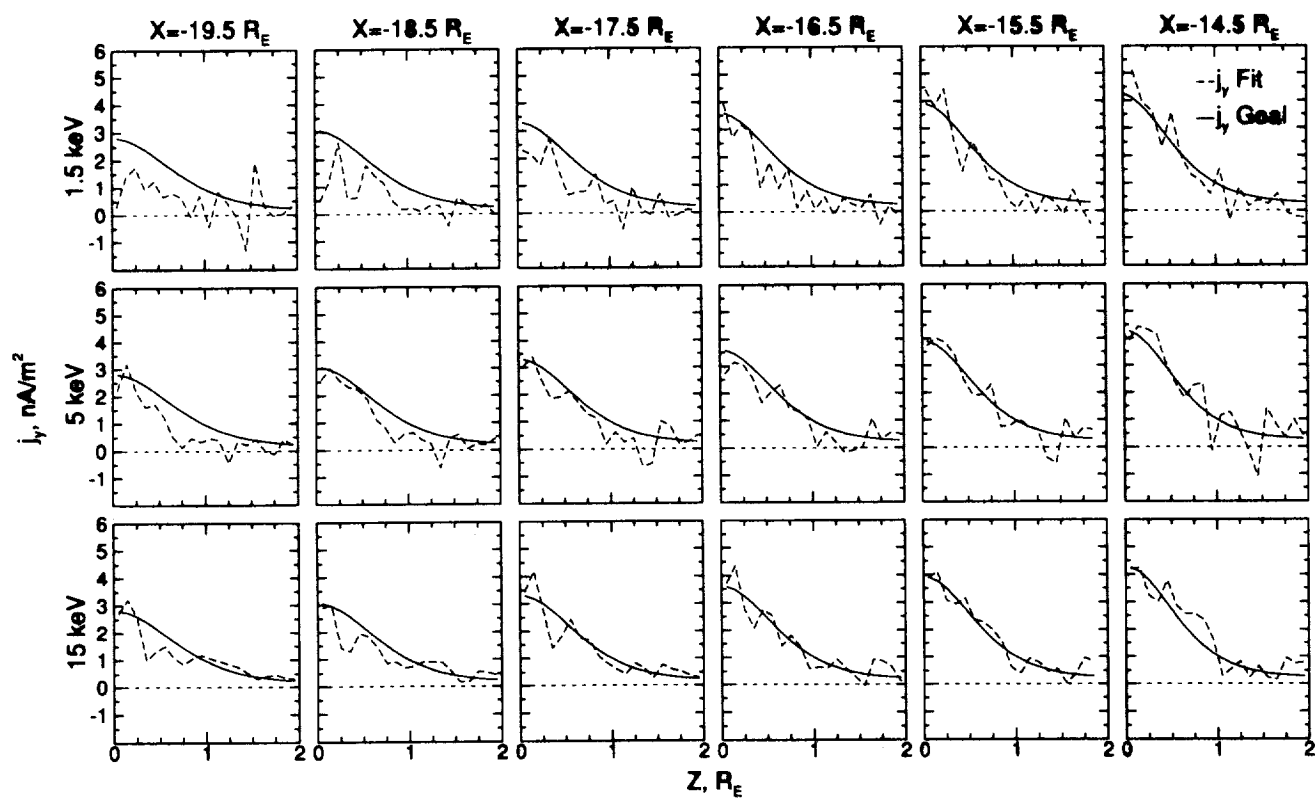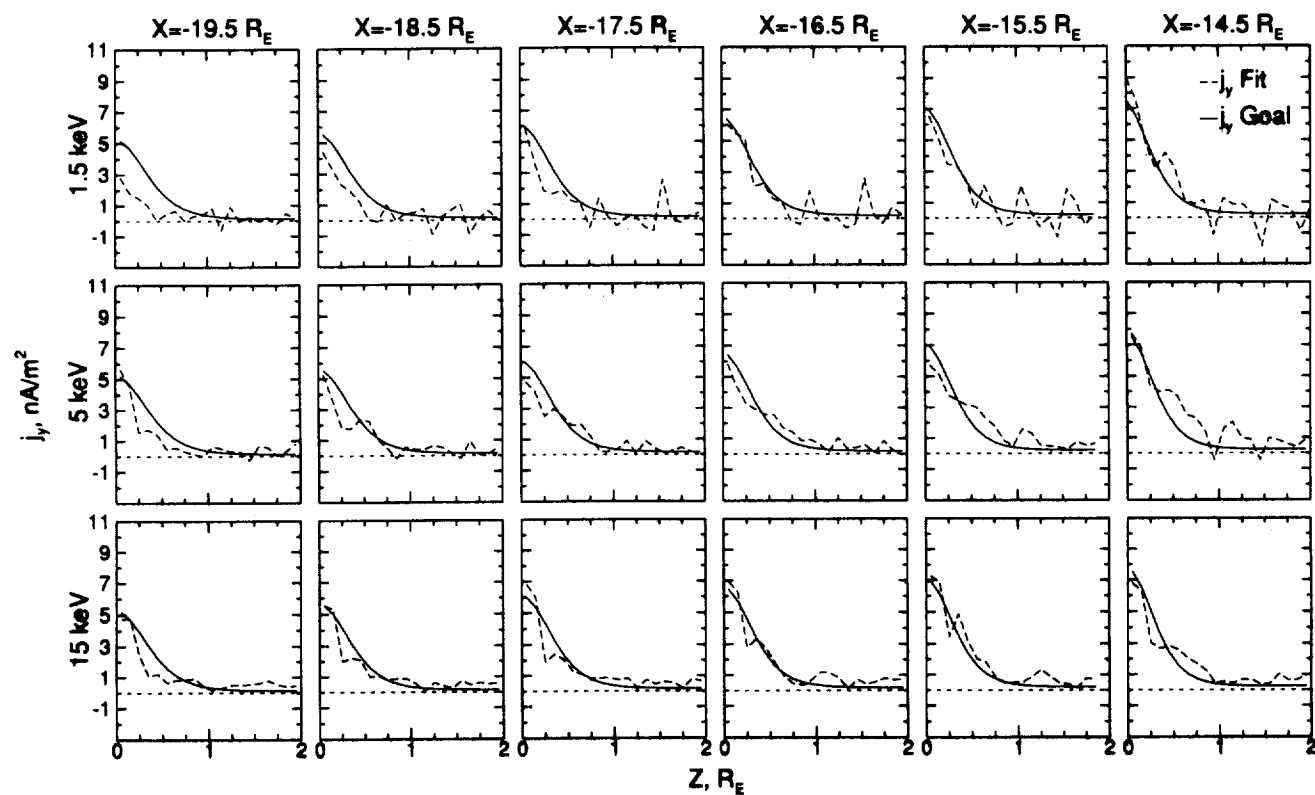**Figure 8.** Similar to Figure 7, except using the standard magnetotail model.

Figure 9. Similar to Figure 7, except using the thin magnetotail model.

everywhere. No such coordinate system exists in a 2-D or 3-D tail if E_y is uniform in the Earth frame.

A different type of problem is caused by our use of monoenergetic particle groups. It is hard to find any completely monoenergetic group that carries significant j_y near $|z| = z_0$. Reasonable fits were found in most cases because there is a substantial spread of energies in the final COT distribution functions, which are weighted sums of five to nine groups. Particles were all started with a given energy, but each group is started at a different location. The energy of each particle changes as it drifts to a desired observation point.

One important result is that, in all nine cases studied, at least one group dominated by each of the three orbit categories that carry distinctive $j_y(x, z)$ distributions had to be retained. The COT technique therefore was unable to generate a current sheet with the desired thickness using generally isotropic ions with the observed energies unless particles mirroring near the Earth, particles trapped near $z = 0$, and particles mirroring throughout the principal current sheet were present. Some 1-D models have been produced using only untrapped particles that are injected at large $|z|$, but the generally isotropic 2-D and 3-D models appear to also require trapped particles and particles with cucumber orbits.

5. Fluid Parameters

A full ion velocity distribution function was saved for each of the 120 spatial boxes. Various moments of $f_i(\mathbf{r}, \mathbf{v})$ were evaluated to calculate the ion density, bulk flow velocity, and other parameters. This section discusses the parameters that are easiest to compare with published satellite measurements. It should be emphasized that the least squares fitting routine that determined which groups to keep used only $j_y(x, z)$ to set weighting factors. The other parameters that were preselected for each run were the magnetic and electric fields, the ion starting energies, an isotropic starting pitch angle distribution, and the 1/7 ratio of electron to ion energies. No other adjustments were made to any of the parameters discussed in this section in an attempt to obtain agreement with observations.

Density and Parallel Electric Fields

The solid lines in Figure 10a are contours of constant $n_i(x, z)$ and the dashed curves are magnetic field lines. *Baumjohann et al.* [1989] binned AMPTE/IRM data according to satellite location and the AE index. The two spatial bins that are most relevant to our model of the current sheet were together referred to as the inner CPS. The region closest to the neutral sheet was defined by $B_{xy} < 7.5$ nT, where $B_{xy}^2 = B_x^2 + B_y^2$, and will be referred to as the inner current sheet. The portion of the inner CPS farther from $z = 0$ was defined by $7.5 < B_{xy} < 15$ nT, and will be referred to as the outer current sheet. The AMPTE/IRM satellite did not make measurements at the statistically averaged location of the neutral sheet [*Fairfield*, 1980] in our region of interest during the 1986 magnetotail data collection periods. However, many neutral sheet crossings were observed when the neutral sheet was displaced from its average location. The entire plasma sheet is known to undergo substantial motion in the z direction. No obvious dependence of plasma parameters upon the neutral sheet displacement from its average location was noted in a brief comparison with 1985 data, which had better orbital coverage. The inner CPS data show an average density of about 0.3 cm^{-3} with little z dependence.

Kistler et al. [1993] sorted AMPTE/IRM data taken at radial distances beyond 15 R_E according to substorm phase and to dis-
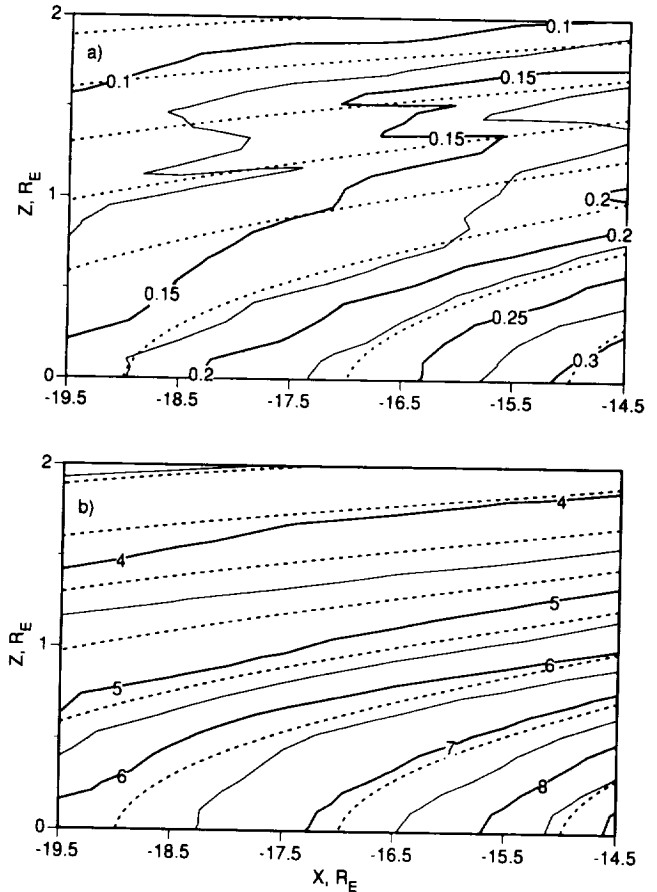

Figure 10. (a) Contour plot of lines of constant density in ions/cm^{-3} for the standard 5-keV model. Dashed curves are magnetic field lines. (b) Contour plot of the average ion energy in keV for the standard 5-keV model.

tance from the neutral sheet. This study used a more complex method to estimate distance from the neutral sheet. The plasma β, or ratio of particle to magnetic field pressures was determined for each data point. The highest β is expected near $z = 0$, and the lowest β in the lobes. Points were binned according to β into 3 groups, labeled inner, middle, and outer plasma sheet. With respect to sorting by substorm phase, it is most reasonable to compare our quiet time model to data taken before substorm onset. Densities were about 0.4 cm^{-3} in the inner and middle third, and about 0.2 cm^{-3} in the outer third of the plasma sheet (L. Kistler, private communication, 1995).

Huang and Frank [1994b] sorted ISEE 1 data according to distance from the *Gosling et al.* [1986] average neutral sheet location. The satellite orbit provided good coverage of this neutral sheet region. The average observed density was approximately 0.25 cm^{-3} during both quiet and disturbed times, with little consistent z dependence.

The above measurements involved statistical averages over a number of orbits. An absolute distance scale was not determined in these statistical treatments. For example, it usually was not known when the satellite was exactly 0.5 R_E, 1.0 R_E, 1.5 R_E, or any other specific distance from the center of the neutral sheet. Only a few analyses have been carried out that determined the instantaneous structure of the current sheet during quiet conditions in our region of interest. These studies measured the current sheet structure using both ISEE 1 and 2 spacecraft. Of these, we could find only

two that also described plasma density and temperature variations within the current sheet. *McComas et al.* [1986] studied three crossings that were associated with the passage of a strong interplanetary shock front. It was concluded that the plasma density, temperature, and pressure changes were consistent with approximate plasma plus magnetic field pressure balance. However, temporal changes in the current sheet structure and orientation were so large during this orbit that it was not possible to determine a consistent density or temperature profile. *Zhou et al.* [1995] found two periods during which a number of current sheet crossings took place with the spacecraft well positioned to measure density and temperature gradients. They concluded that both density and temperature decreased by a factor of two as the spacecraft moved 1.5 current sheet thickness scale lengths from $z = 0$. The average half thicknesses on this orbit were $2\ R_E$ when the IMF pointed northward and $0.5\ R_E$ when the IMF pointed southward.

The COT standard 5-keV model number densities nearest the neutral sheet (Figure 10a) are close to or slightly below the observed values. The dropoff of $n\ (x, z)$ with increasing z is similar to that measured by *Zhou et al.* [1995] but more rapid than the dropoff suggested by the statistical studies. The model density depends on the starting ion energies used. Densities for the standard model were 3 to 4 times larger when 1.5-keV protons were used instead of 5-keV protons, and about half as large as in Figure 10a when 15-keV protons were used. The density in the thick model with 5-keV protons was similar to that in Figure 10a, while densities near $z = 0$ were about 50% larger in the thin 5-keV model. Our earlier self-consistent 1-D model used 3-keV protons [*Kaufmann and Lu*, 1993] and required particle densities as high as the 2-D model with 1.5-keV protons.

Figure 10a shows that the model ion density is nearly constant along magnetic field lines near $z = 0$, and that the density increases slowly as one moves earthward along a field line beyond $z = 1.5$ R_E. However, the density increases rapidly as one moves earthward in the $1\ R_E < z < 1.5\ R_E$ region. As described previously, charge neutrality was maintained in the model consisting of isotropic electrons and nonguiding center ions by introducing a parallel electric field. Very abrupt changes would be required in the equatorial pitch angle distribution of electrons on these field lines if the equally rapid drop in electron density that is needed to maintain charge neutrality were to be produced by mirror effects with $E_{||} = 0$. The density changes seen along field lines at $z < 1\ R_E$ and at $z > 1.5\ R_E$ in Figure 10a were typical of the changes seen throughout the region of interest for the other eight cases studied. No other case showed as large a field-aligned density drop as that seen at 1 $R_E < z < 1.5\ R_E$ in Figure 10a.

Thermal Energies

Figure 10b shows the average ion energy for the standard 5-keV model. *Baumjohann et al.* [1989] observed an average inner plasma sheet temperature of 4 keV in the region of interest, with slightly lower values during quiet times. *Huang and Frank* [1994b] found average temperatures of 3-4 keV during quiet times, and up to 7 keV during disturbed times. The temperature was higher in the inner than in the outer plasma sheet. L. Kistler (private communication, 1995) found temperatures dropping from 4 keV in the inner plasma sheet to 2 keV in the outer plasma sheet before substorms. *Zhou et al.* [1995] found approximately a factor of two drop in temperature when moving 1.5 thickness scale lengths from $z = 0$. A temperature of 4 keV corresponds to an average ion energy of $3/2$ $T = 6$ keV. Figure 10b shows average energies rather than temperatures because monoenergetic groups were used.

The calculated average energy in the region of interest dropped from about 7 keV to about 3.5 keV, which is close to the observed temperature variation. Since the starting ion energy is one of the preselected parameters, the average energy in the model can easily be changed. As noted above, lower energies will increase the required density, so a small decrease in the starting energy to below 5 keV would slightly improve the agreement with both the measured $n\ (x, z)$ and $T\ (x, z)$.

The observed plasma β or particle/field energy density ratio [*Baumjohann et al.*, 1989] dropped from approximately 20 in the neutral sheet region to 3 in the outer current sheet, and to 0.3 in the outer plasma sheet. Results from all nine of the cases studied here showed decreases from $\beta = 20$ - 100 at $z = 0$ to $\beta = 0.1$ - 0.5 at $z = 2$ R_E. The detailed dropoff depended weakly on the particle energy and magnetic field models used. All cases therefore showed reasonable agreement with observations.

Bulk Flow

Finally, Figure 11 shows the model ion bulk flow velocity

$$V_{i\alpha}(\mathbf{r}) = (1/n) \int v_\alpha\, f_i(\mathbf{r}, \mathbf{v})\, d^3v \qquad (4)$$

Detailed examination of $f_i(\mathbf{r}, \mathbf{v})$ shows that two features contribute to this bulk flow. The principal cause of V_{iy} is an asymmetry in the nearly monoenergetic spherical phase space shell of ions in our model. Ions going to the east and west have the same energies, but there are more going westward. This behavior is associated with the large westward displacement of ions, especially near $z = 0$, that is evident in Figures 2 and 3. This net positive V_{iy} produces most of the cross-tail current, with eastward electron drift causing the rest. It is interesting to note that the model V_{iy} carried by a realistic particle distribution decreases with increasing $|z|$ even though the dominant equilibrium tail field module was developed using a uniform V_{iy}.

The nature of V_{ix} shown in Figure 11 is substantially different. This component is primarily field aligned except very near $z = 0$, where V_{ix} is mostly $\mathbf{E} \times \mathbf{B}$ drift. The model distribution function away from $z = 0$ shows that the entire spherical shell experiences a net shift in the positive V_{ix} direction, so that ions moving earthward are slightly more energetic than are those moving tailward. A less important angular asymmetry also is sometimes seen in the opposite direction, with a larger number of ions moving tailward than earthward. This small angular asymmetry reduces the net earthward V_{ix}, particularly near $z = 1\ R_E$ in Figure 11. A decrease in V_{ix} somewhere near $z = 1\ R_E$ was seen in most of the nine cases studied. A positive V_{ix} is commonly seen in our region of interest in both AMPTE/IRM [*Baumjohann et al.*, 1989] and ISEE 1 [*Huang and Frank*, 1994b] data.

In a 1-D model, the uniform $E_y = 0.3$ mV/m field is transformed to zero in the deHoffman Teller reference frame which moves earthward at a speed E_y/B_{zo}. The z component of $\mathbf{B}$ is uniform in a 1-D model. There is no reference frame in which this uniform E_y is transformed to zero everywhere in 2-D or 3-D models. Ions near $z = -19.5\ R_E$ in the nine models used here drift earthward at a speed that is about 25% less than E_y/B_{zo} based on B_z at $z = 0$. The speed E_y/B_{zo} at $x = -19.5\ R_E$ is about 140, 120, and 85 km/s in the thick, standard, and thin models, respectively. At $x = -14.5\ R_E$, the model V_{ix} was only about 10% less than E_y/B_{zo}, which equaled 85, 75, and 65 km/s respectively in the three models. We therefore conclude that E_y/B_{zo} produces approximate but not accurate estimates of V_{ix} in 2-D or 3-D models.
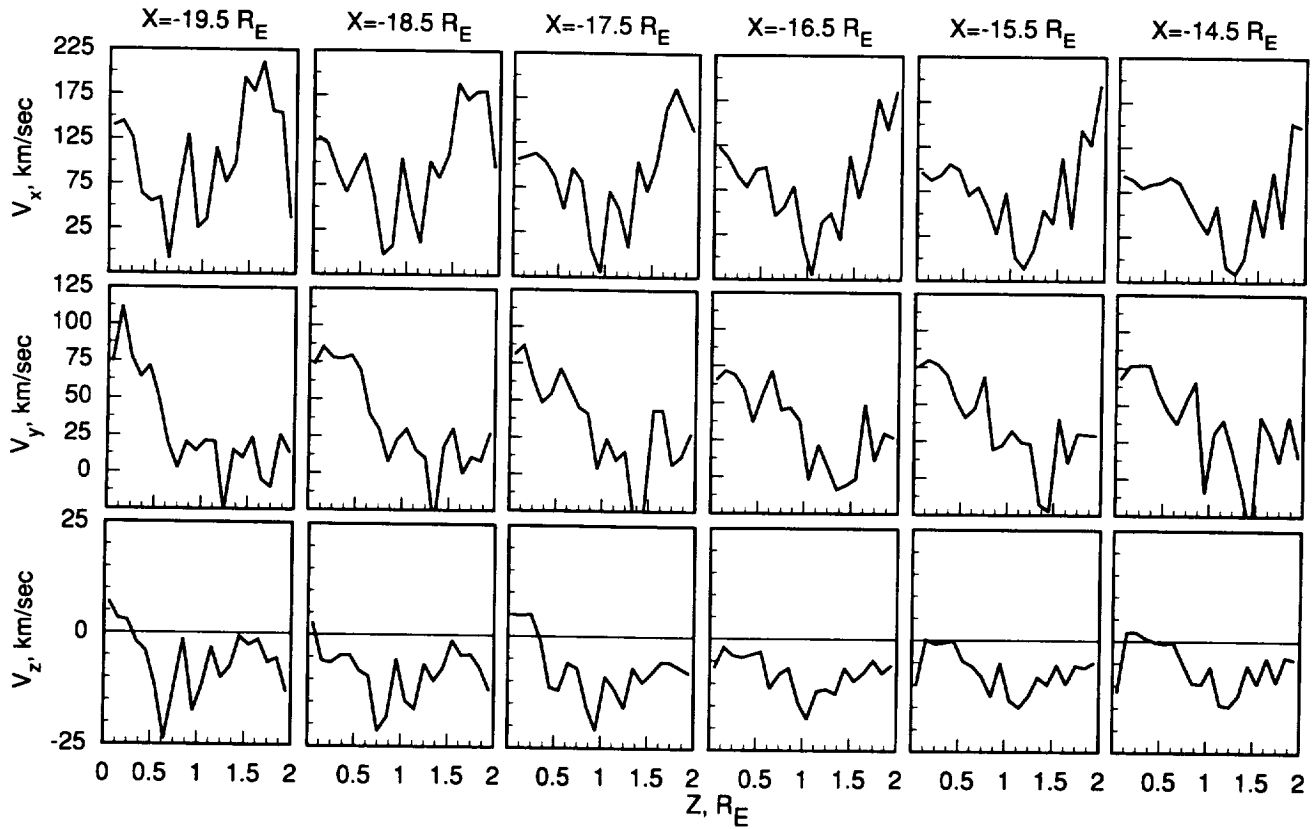
Figure 11. The x, y, and z components of the ion bulk velocity for the standard 5-keV model.

The single particle orbits show the physical origin of the strong field-aligned drift. The effect is produced primarily by ions that mirror within the current sheet. For example, the ion in Figure 2a moved approximately 5 R_E earthward, generally along B, as it went from $x = -19$ R_E, $z = 0.5$ R_E to a mirror point at $x = -14$ R_E. The ion then moved only about 2.5 R_E tailward from the mirror point, primarily along B, until it returned to $z = 0.5$ R_E. The net 2.5 R_E earthward motion at $z > 0.5$ R_E contributes to a generally field-aligned bulk flow. Other examples are evident in Figures 2c and 3a.

A small net drift toward $z = 0$ is seen in the model V_{iz}. This is primarily E × B drift in the negative z direction, though field-aligned drift also provides a positive contribution to V_z. The model $E_y = 0.3$ mV/m electric field produces a 20 km/s drift toward $z = 0$ in a region with $B_x = 15$ nT. Electrons and ions E × B drift in the same direction, so these contributions to the current tend to cancel in the outer current sheet, where the guiding center approximations are valid.

Although it does not affect the COT analysis, which is based only on j_y, electrons were assumed to drift along field lines at the same speed as ions. This assumption was needed to make $\nabla \cdot \mathbf{j} = 0$ for electrons, and also so there would be no Birkeland current. No field aligned current is expected in the present steady state model with essentially no y dependence in the region of interest.

6. Discussion and Summary

The Consistent Orbit Tracing (COT) technique was described. The principal steps were: select a number of proton groups, trace orbits of the 1000 protons in each group, evaluate the cross-tail current carried by each group of ions plus their associated elec-

trons, and combine these groups so that they produce a nearly consistent current sheet. In a consistent current sheet, the ions and electrons carry the current needed to generate the magnetic field in which the orbits were traced.

A set of nine COT analyses were carried out using 3 proton energies (1.5, 5, and 15 keV) for each of three magnetic field models. Characteristic current sheet thickness scale lengths varied from 0.3 R_E to 1 R_E in the models used. Selection of these thicknesses was guided by the few available observations of the instantaneous structure of a steady magnetotail current sheet. The adiabaticity parameter κ ranged from 0.3 to 0.65 in the -20 $R_E < x < -14$ R_E region of interest. A uniform zeroth order cross-tail electric field was present in all calculations. A first order parallel electric field was added to maintain charge neutrality.

An earlier study using a 1-D modified Harris magnetic field model [*Kaufmann and Lu*, 1993] was unable to generate a current sheet that agreed with observations in the region of interest. The introduction of a 2-D equilibrium tail module, which has both x and z dependence, removed the inconsistencies found in the earlier 1-D analysis. It was possible to generate nearly consistent current sheets for most of the magnetic field model and particle energy combinations. Adequate solutions were not found when attempting to combine the thicker model current sheets and ions with energies that were lower than those typically observed in the region of interest.

The results of this analysis support the postulate that in sheet-like structures, current is carried mostly by particles with $B_{zo}/B_{xo} < \kappa < 1$, where B_{xo} is B_x in the lobes and B_{zo} is B_z at $z = 0$. The lower limit on κ is needed for consistency in a modified Harris 1-D model field. It is based on the need to confine current within the current sheet in any consistent model. In the present

study we found it difficult to create a consistent current sheet using particles with $\kappa > 1$. The ring current magnetic field is generated primarily by particles inside the Earth, so $\kappa > 1$ particles can dominate in the radiation belts.

Burkhart et al. [1992] carried out a consistent orbit tracing study for a 1-D magnetotail. Their treatment was different from that used here in that it involved a fixed source of particles injected at the edge of the current sheet. The magnetic field was allowed to change until consistency was attained. The model therefore had few trapped particles. The resulting current sheets were very thin, with small κ and a scale size of approximately z_0. *Burkhart et al.* [1992] concluded that this type of current sheet could not be generated when κ approached 1.

Ashour-Abdalla et al. [1993, 1995] used a 2-D version of the T89 model for a series of orbit tracing studies. They used a fixed source in the mantle for these large-scale kinetic (LSK) models. A goal was to demonstrate that a reasonable magnetotail could be generated using only a mantle source. The particles were followed as they drifted all the way in from the distant tail through our region of interest. There were so many chaotic interactions with the current sheet that all orbit categories became populated by the time particles reached our region of interest.

The final model was found to be nearly in force balance, even though the model was not really consistent because both the particle source and the basic fields were preselected. Calculated currents tended to be carried in a sheet that is thinner than would be needed to generate the T89 field. The density profile was qualitatively similar to our Figure 10a, though the drop-off in z was slower than in our results. Earthward drift was slower than in our model because the LSK calculations were run with an 0.1 mV/m cross-tail field, while our COT calculations used 0.3 mV/m. The cross-tail drift velocities were comparable in the two models, as is required to support the comparable lobe fields.

A principal goal of the present study was to use individual particle orbits to better understand how particles carry current in a sheet-like structure. All ions in each group were started with the same energy so that the group would be dominated by a particular type of orbit. Particle orbits previously have been classified according to the dynamical properties of the particles. Guiding center, chaotic, and resonant orbits are examples. Instead, orbits in this work were grouped according to the characteristic spatial distribution of cross-tail current carried by the particles. This resulted in three orbit categories: particles that remain near $z = 0$ (trapped orbits), particles that spiral and then magnetically mirror elsewhere in the principal current sheet (cucumber orbits), and particles that magnetically mirror closer to Earth (Speiser orbits). Consistent current sheets required the use of all three orbit categories in each of the nine cases studied.

A study of single ion orbits showed the features that resulted in the characteristic $j_y(x, z)$ pattern carried by particles in each orbit category. Magnetization currents produced most of the structure and characteristic scale of the magnetotail current sheet. Substantial earthward drift was found in the COT results. This was attributed to particles mirroring within the current sheet. Such particles were seen to drift farther earthward than tailward along field lines during a bounce period.

A number of assumptions were introduced in order to include electrons. Some of these assumptions were needed to satisfy basic requirements of the steady state model, such as charge neutrality and conservation. Other assumptions, such as the ratio of electron to ion energy, were based on observations. Electrons with the energies used here obeyed the guiding center approximations throughout the region of interest in all three magnetic field models.

Cross-tail electron currents were relatively small in the model current sheets studied here. Electron current can be much more important in a thinner current sheet. Extremely thin current sheets have been observed just before and just after substorm onsets [*Mitchell et al.*, 1990; *Sergeev et al.*, 1993; *Hesse et al.*, 1995; *Pritchett and Coroniti*, 1995]. The present work did not attempt to model such situations.

The COT analysis produced an ion distribution function for each of the 120 spatial boxes used in this study. The distribution functions were integrated to evaluate fluid parameters. Three of the simplest parameters: the ion density, temperature, and bulk flow velocity, were in good agreement with observations. Comparisons of other fluid parameters, a study of force balance, and an analysis of energy fluxes will be presented in the future.

References

Ashour-Abdalla, M., L. M. Zelenyi, J. M. Bosqued, V. Peroomian, Z. Wang, D. Schriver, and R. L. Richard, The formation of the wall region: Consequences in the near earth magnetotail, *Geophys. Res. Lett.*, *19*, 1739-1742, 1992.

Ashour-Abdalla, M., J. P. Berchem, J. Büchner, and L. M. Zelenyi, Shaping of the magnetotail from the mantle: Global and local structuring, *J. Geophys. Res.*, *98*, 5651-5676, 1993.

Ashour-Abdalla, M., L. M. Zelenyi, V. Peroomian, R. L. Richard, and J. M. Bosqued, The mosaic structure of plasma bulk flows in the Earth's magnetotail, *J. Geophys. Res.*, *100*, 19,191-19,209, 1995.

Baumjohann, W., G. Paschmann, and C. A. Cattell, Average plasma properties in the central plasma sheet, *J. Geophys. Res.*, *94*, 6597-6606, 1989.

Bernstein, I. B., J. M. Greene, and M. D. Kruskal, Exact nonlinear plasma oscillations, *Phys. Rev.*, *108*, 546-550, 1957.

Bird, M. K., and D. B. Beard, The self-consistent geomagnetic tail under static conditions, *Planet. Space Sci.*, *20*, 2057-2072, 1972.

Birn, J., R. Sommer, and K. Schindler, Open and closed magnetospheric tail configurations and their stability, *Astrophys. Space Sci.*, *35*, 389-402, 1975.

Büchner, J., and L. M. Zelenyi, Regular and chaotic charged particle motion in magnetotaillike field reversals, 1, Basic theory of trapped motion, *J. Geophys. Res.*, *94*, 11,821-11,842, 1989.

Burkhart, G. R., and J. Chen, Particle motion in x-dependent Harris-like magnetotail models, *J. Geophys. Res.*, *98*, 89-97, 1993.

Burkhart, G. R., J. F. Drake, P. B. Dusenbery, and T. W. Speiser, A particle model for magnetotail neutral sheet equilibria, *J. Geophys. Res.*, *97*, 13,799-13,815, 1992.

Chen, J., Nonlinear dynamics of charged particles in the magnetotail, *J. Geophys. Res.*, *97*, 15,011-15,050, 1992.

Cowley, S. W. H., A note on the motion of charged particles in one-dimensional magnetic current sheets, *Planet. Space Sci.*, *26*, 539-545, 1978.

Eastwood, J. W., Consistency of fields and particle motion in the 'Speiser' model of the current sheet, *Planet. Space Sci.*, *20*, 1555-1568, 1972.

Fairfield, D. H., A statistical determination of the shape and position of the geomagnetic neutral sheet, *J. Geophys. Res.*, *85*, 775-780, 1980.

Fairfield, D. H., The magnetic field of the equatorial magnetotail from 10 to 40 R_E, *J. Geophys. Res.*, *91*, 4238-4244, 1986.

Gosling, J. T., D. J. McComas, M. F. Thomsen, S. J. Bame, and C. T. Russell, The warped neutral sheet and plasma sheet in the near-Earth geomagnetic tail, *J. Geophys. Res.*, *91*, 7093-7099, 1986.

Hada, T., A. Nishida, T. Terasawa, and E. W. Hones Jr., Bi-directional electron pitch angle anisotropy in the plasma sheet, *J. Geophys. Res.*, *86*, 11,211-11,224, 1981.

Harris, E. G., On a plasma sheath separating regions of oppositely directed magnetic field, *Il Nuovo Cimento, 23,* 115-121, 1962.

Hesse, M., D. Winske, and M. M, Kuznetsova, Hybrid modeling of collisionless reconnection in two-dimensional current sheets: Simulations, *J. Geophys. Res., 100,* 21,815-21,825, 1995.

Huang, C. Y., and L. A. Frank, Magnitude of B_z in the neutral sheet of the magnetotail, *J. Geophys. Res., 99,* 73-82, 1994a.

Huang, C. Y., and L. A. Frank, A statistical survey of the central plasma sheet, *J. Geophys. Res., 99,* 83-95, 1994b.

Kan, J. R., On the structure of the magnetotail current sheet, *J. Geophys. Res., 78,* 3773-3781, 1973.

Karimabadi, H., P. L. Pritchett, and F. V. Coroniti, Particle orbits in two-dimensional equilibrium models for the magnetotail, *J. Geophys. Res., 95,* 17,153-17,166, 1990.

Kaufmann, R. L., and C. Lu, Magnetotail current carriers: Quasiadiabatic orbits, *J. Geophys. Res., 98,* 15,447-15,465, 1993.

Kistler, L. M., W. Baumjohann, T. Nagai, and E. Möbius, Superposed epoch analysis of pressure and magnetic field configuration changes in the plasma sheet, *J. Geophys. Res., 98,* 9249-9258, 1993.

Mitchell, D. G., D. J. Williams, C. Y. Huang, L. A. Frank, and C. T. Russell, Current carriers in the near-Earth cross-tail current sheet during substorm growth phase, *Geophys. Res. Lett., 17,* 583-586, 1990.

McComas, D. J., C. T. Russell, R. C. Elphic, and S. J. Bame, The near-Earth cross-tail current sheet: Detailed ISEE 1 and 2 case studies, *J. Geophys. Res., 91,* 4287-4301, 1986.

Nakamura, M., G. Paschmann, W. Baumjohann, and N. Sckopke, Ion distributions and flows near the neutral sheet, *J. Geophys. Res., 96,* 5631-5649, 1991.

Paterson, W. R., L. A. Frank, S. Kokubun, T. Yamamoto, and R. P. Lepping, Geotail observations of magnetospheric currents (abstract), *EOS Trans. AGU, 76,* Fall Meet. Suppl., F485, 1995.

Pritchett, P. L, and F. V. Coroniti, Formation of thin current sheets during plasma sheet convection, *J. Geophys. Res., 100,* 23,551-23,565, 1995.

Rich, F. J., V. M. Vasyliunas, and R. A. Wolf, On the balance of stresses in the plasma sheet, *J. Geophys. Res., 77,* 4670-4676, 1972.

Rostoker, G., and S. Skone, Magnetic flux mapping considerations in the auroral oval and the Earth's magnetotail, *J. Geophys. Res., 98,* 1377-1384, 1993.

Sanny, J., R. L. McPherron, C. T. Russell, D. N. Baker, T. I. Pulkkinen, and A. Nishida, Growth-phase thinning of the near-Earth current sheet during the CDAW 6 substorm, *J. Geophys. Res., 99,* 5805-5816, 1994.

Schindler, K, A self-consistent theory of the tail of the magnetosphere, in *Earth's Magnetospheric Processes,* edited by B. M. McCormac, pp. 200-209, D. Reidel, Norwell, Mass., 1972.

Sergeev, V. A., D. G. Mitchell, C. T. Russell, and D. J. Williams, Structure of the tail plasma/current sheet at ~11 R_E and its changes in the course of a substorm, *J. Geophys. Res., 98,* 17,345-17,365, 1993.

Speiser, T. W., Particle trajectories in model current sheets. 1. Analytic solutions, *J. Geophys. Res., 70,* 4219-4226, 1965.

Stern, D. P., and P. Palmadesso, Drift-free magnetic geometries in adiabatic motion, *J. Geophys. Res., 80,* 4244-4248, 1975.

Tsyganenko, N. A., A magnetospheric magnetic field model with a warped tail current sheet, *Planet. Space Sci., 37,* 5-20, 1989.

Tsyganenko, N. A., and A. V. Usmanov, Determination of the magnetospheric current system parameters and development of experimental geomagnetic field models based on data from IMP and HEOS satellites, *Planet. Space Sci., 30,* 985-998, 1982.

Zhou, X. -Y., C. T. Russell, and J. T. Gosling, Three spacecraft observations of the geomagnetic tail during moderately disturbed conditions: Inferences from a Harris current sheet model (abstract), *EOS Trans. AGU, 76,* Fall Meet. Suppl., F492, 1995.

Zwingmann, W., Self-consistent magnetotail theory: Equilibrium structures including arbitrary variation along the tail axis, *J. Geophys. Res., 88,* 9101-9108, 1983.

R. L. Kaufmann and D. J. Larson, Department of Physics, DeMeritt Hall, 9 Library Way, University of New Hampshire, Durham, NH 03824-3568. (e-mail: dick.kaufmann@unh.edu; djl@sppsgi.unh.edu)